

QoS Provisioning in 60 GHz Communications by Physical and Transport Layer Coordination

Matteo Drago^o, Michele Polese^o, Stepan Kucera[†], Dmitry Kozlov[†], Vitalii Kirillov[†], Michele Zorzi^o

^oUniversity of Padova, Padova, Italy - {dragomat, polesemi, zorzi}@dei.unipd.it

[†]Nokia Bell Labs, Dublin, Ireland - {stepan.kucera, dmitry.1.kozlov}@nokia-bell-labs.com

vitalii.1.kirillov@nokia.com

Abstract—In the last decades, technological developments in wireless communications have been coupled with an increasing demand of mobile services. From real-time applications with focus on entertainment (e.g., high quality video streaming, virtual and augmented reality), to industrial automation and security scenarios (e.g., video surveillance), the requirements are constantly pushing the limits of communication hardware and software. Communications at millimeter wave frequencies could provide very high throughput and low latency, thanks to the large chunks of available bandwidth, but operating at such high frequencies introduces new challenges in terms of channel reliability, which eventually impact the overall end-to-end performance. In this paper, we introduce a proxy that coordinates the physical and transport layers to seamlessly adapt to the variable channel conditions and avoid performance degradation (i.e., latency spikes or low throughput). We study the performance of the proposed solution using a simulated IEEE 802.11ad-compliant network, with the integration of input traces generated from measurements from real devices, and show that the proposed proxy-based mechanism reduces the latency by up to 50% with respect to TCP CUBIC on a 60 GHz link.

Index Terms—5G, mmWave, reliability, transport.

I. INTRODUCTION

The next generations of wireless networks are being designed to address the needs and use cases of the digital society for the next decade, with an ever increasing number of connected devices and multimedia traffic that will drive the demand for wireless capacity [1]. Additionally, future wireless networks will serve new verticals that so far have generally relied on wired communications, such as, for example, industrial automation, in order to provide lower deployment costs, re-configurability of the factory and flexibility in the mobility of the equipment [2]. This vertical introduces demanding constraints to the wireless communication stack, and a number of studies have focused on how to guarantee the combination of high reliability and low latency required on the factory floor [3], [4].

Recently, millimeter waves (mmWaves) have emerged as an enabler of ultra-high data rate communications, thanks to the massive amount of bandwidth available in the spectrum between 30 and 300 GHz [5]. Operations at such high frequencies are now considered in multiple standards for commercial devices, such as 3GPP NR [6] for cellular networks and IEEE 802.11ad and 802.11ay [7], [8] for wireless Local Area Networks (LANs). The potential of this communication technology has also sparked interest for the aforementioned

industrial automation use case. The authors of [9], [10] consider mmWaves as an enabling technology for future factories, thanks to the reduced interference, the small form factor of the antennas and the multi-gigabit-per-second throughput, which would allow high quality video, telemetry streaming, and low-latency sensing and actuation.

Nonetheless, communication at such high frequencies comes with a set of challenges that must be solved before the deployment in performance-critical scenarios. The main issues are related to the intermittency of the channel, which is easily blocked and/or reflected by common materials, such as metals, brick and mortar [11], as well as the human body, which can cause an attenuation that ranges from 15 dB (hand blockage) [12] to 35 dB (complete body blockage) [13]. Consequently, the mobility of the communication endpoints and of the obstacles and reflectors on a factory floor may cause the channel to disappear, with sudden transitions from Line of Sight (LOS) to Non Line of Sight (NLOS) which may happen in a time interval shorter than 100 ms [14]. Moreover, mmWaves are affected by a high isotropic propagation loss, which increases with the carrier frequency [11].

These issues can be addressed with a combination of high density deployments, which decrease the average distance between a user and an access point and provide macro diversity [15], and directional communications, which compensate the isotropic pathloss thanks to the beamforming gain [16]. These solutions, however, have introduced a paradigm shift in the design of the wireless protocol stack, given that (i) the coverage area of a cell is now limited (thus introducing the need for smart mobility management due to the possibly high number of handovers) [17] and (ii) the endpoints of the communication need to track the optimal beam to be used to transmit and receive data [18].

Additionally, the intermittent mmWave channel has an impact also on the higher layers of the protocol stack and, eventually, on the end-to-end performance of the network. This has been assessed by a number of simulation-based studies [19]–[21], which highlight how the highly variable channel and the LOS to NLOS transition may affect the Transmission Control Protocol (TCP) performance, either by reducing the throughput experienced at the application layer, thus wasting the resources available at mmWaves, or by introducing jitter and bufferbloat (i.e., latency spikes caused by excessive buffering) [22]. The cross-layer interactions between the mmWave channel and the various layers of the protocol

stack thus make the end-to-end performance sub-optimal and unpredictable, impacting the Quality of Service (QoS) of the mmWave flows. This has negative consequences not only on the user experience in mobile networks, but also, most importantly, on the reliability and end-to-end latency that this wireless technology can guarantee in an industrial automation context.

Therefore, in this paper we propose a cross-layer approach to improve the end-to-end performance of mmWave networks, which manages to limit the latency spikes and the throughput drops and thus makes it possible to satisfy tight QoS constraints. The contributions of this paper are two-fold:

- we propose a proxy design for 60 GHz wireless networks, that exploits cross-layer information to discipline the TCP behavior, with two different control policies;
- we evaluate the performance of a baseline and of the proposed solution using real channel measurements at 60 GHz to drive a custom 802.11ad-based physical layer implementation in ns-3. To the best of our knowledge, this is the first study that evaluates TCP performance at 60 GHz using a mixture of simulation and experimentation, thus bridging the gap between purely testbed-based analysis (in which it is often not possible to carefully control and update the parameters of the protocol stack) [23] and the aforementioned simulation-based evaluations [20].

The results show that implementing a cross-layer strategy with periodical reports could yield a reduction of up to 50% in terms of latency, and more than double the performance in terms of throughput.

The remainder of the paper is organized as follows. In Section II we review the state of the art on transport layer performance in mmWave networks. Then, in Section III, we present the proxy mechanism that we introduce to enable physical and transport layer coordination. In Section IV we describe the mixed experimental- and simulation-based evaluation setup, which is then used to obtain the results we discuss in Sec. V. Finally, we conclude the paper and suggest possible extensions in Sec. VI.

II. TRANSPORT LAYER PERFORMANCE AT MMWAVES

As mentioned in Section I, communications at mmWave frequencies can provide gigabit-per-second data rates at the physical layer, thanks to the large chunks of spectrum that are available in these bands [5].

The end-to-end performance of mmWave cellular networks has been recently in the spotlight thanks to mostly simulation studies [19]–[21], [24]–[26], using the end-to-end mmWave module of ns-3 [27], and to some preliminary testbed-based evaluations [23], [28]. The studies have mainly focused on understanding the pitfalls that prevent TCP from delivering high throughput and low latency to the application layer. The first results were presented in [19], [21], where the authors show how TCP is too slow to react to the dynamics of the underlying mmWave channel, because of its abstract view of the end-to-end connection. The TCP-related problems that these studies highlight are the slow ramp up of the TCP

congestion window, which leads to a sub-optimal resource utilization, the emergence of high latency spikes after LOS to NLOS transitions, and the possibility of extended outages that trigger retransmission timeouts.

The first issue is linked to how the most widely used TCP congestion control algorithms (e.g., TCP CUBIC [29] and TCP NewReno [30]) update their congestion window in the congestion avoidance phase, i.e., with a linear growth that takes too long to reach the full capacity offered by the channel [19].

The second issue is related to the appearance of bufferbloat in end-to-end connections where the Radio Access Network (RAN) link is operated at mmWave frequencies [21], [24], with a protocol stack for the wireless link that performs buffering (as in IEEE 802.11ad [31] and 3GPP NR [32]). Buffering strategies are fundamental to protect against sudden swings in the channel quality that affect the physical layer capacity, and, as highlighted in [19], an undersized buffer may lead to high packet loss when the channel is in NLOS and, consequently, to severe throughput degradation. On the other hand, an oversized buffer, while protecting from these losses, thus preventing negative consequences on the throughput, at the same time makes TCP unaware of the dynamics in the available capacity, at least until one or more packets are dropped or an Active Queue Management (AQM) procedure is triggered. Therefore, TCP keeps sending data at a rate higher than that supported by the channel, which results in an end-to-end latency increase due to excessive buffering. As discussed in [20], the oversized buffer solution yields higher throughput but, at the same time, the highest average end-to-end latency for the TCP flows. The deployment of AQM in the buffers of the base stations represents an intermediate solution, which however does not guarantee the best performance in terms of either throughput or latency [20].

Finally, the third issue is caused by the possibility of extended channel outages, i.e., if there is no alternative path when the communication link is blocked. In this case, TCP may react by triggering multiple retransmission timeouts. Upon each timeout, TCP halves the slow start threshold so that, when the link is re-established, the slow start phase (in which the congestion window grows exponentially) has a limited duration and TCP quickly transitions to congestion avoidance, thus aggravating the inefficiency associated to the slow ramp up of the congestion window.

The research community has also highlighted a number of possible solutions to allow TCP to harness the potential of mmWave communications. In [20], the authors propose to increase the Maximum Segment Size (MSS) of the TCP flow in order to speed up the growth of the congestion window. This, however, may not be feasible in end-to-end flows that traverse Ethernet links, where the MSS should be limited to the Ethernet Maximum Transmission Unit (MTU) of 1500 bytes. Moreover, in some applications that require low latency it is not possible to aggregate enough data to create large packets. In [21], [26], multipath solutions and mobility management are used to provide macro diversity, thus decreasing the probability

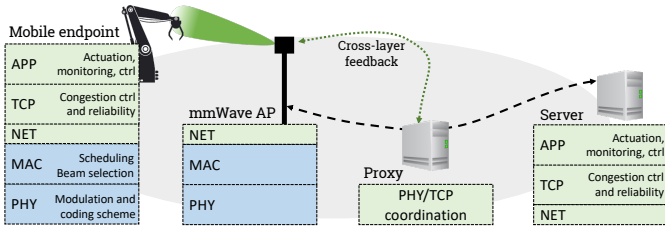


Fig. 1: Factory architecture with mmWave access point and proxy.

of a LOS to NLOS transition. However, multiple backup links may not be available in all scenarios, especially when the density of the deployment is low or when the environment has few reflections. Finally, the authors of [33], [34] propose to implement a proxy in the cellular network architecture (either in base stations or at the edge of the network) that exploits cross-layer information to steer the behavior of TCP. While [33] aims at transparently forcing the TCP congestion window to track the connection bandwidth delay product, the authors of [34] also introduce an additional layer of retransmissions to protect the TCP sender from receiving duplicate acknowledgments. Finally, [35] adopts a similar approach for uplink flows, by modifying the protocol stack in the User Equipment (UE) which acts as TCP sender.

With respect to the the studies reviewed in this section, in this paper we assess the performance of TCP over 60 GHz links using the ns-3 simulator with real traces from an indoor environment, and propose two proxy policies that aim at enforcing QoS constraints (i.e., high throughput with low latency) over IEEE 802.11ad-based links.

III. PHYSICAL AND TRANSPORT LAYER COORDINATION

This section describes the proposed physical and transport layer coordination mechanism, along with the cross-layer policies that are implemented in the proxy. An example of the scenario of interest is shown in Figure 1, where a mmWave Access Point (AP) at 60 GHz provides connectivity to mobile and static factory equipment, and a proxy is added to improve the performance of the end-to-end flows. The access point provides physical and Medium Access Control (MAC) layer functionalities which are similar in the main protocol stacks proposed for mmWave operations (i.e., 3GPP NR and IEEE 802.11ad/ay). In particular, the most relevant in the context of this work are Adaptive Modulation and Coding (AMC) at the physical layer, which dictates the data rate that the wireless network offers to the higher layers, according to the experienced channel quality, and beam selection and scheduling (or medium access) at the MAC layer.

The proxy coordinates the Physical (PHY), MAC and transport layers to efficiently exploit the available network resources. We would like to remark that the framework presented in this section is generic and can be applied to any wireless protocol stack that offers the aforementioned capabilities. In particular, the cross-layer exchange involves the following operations:

- the mobile device periodically collects a matrix representing the channel quality (e.g., the received power, or Signal to Noise Ratio (SNR)) over the available transmitter and receiver beam pairs $(b_{tx}, b_{rx}) \in \mathcal{B}_{tx} \times \mathcal{B}_{rx}$, where \mathcal{B}_i represents the set of directions that an endpoint considers (for pilot transmission at the AP and monitoring at the mobile device). This information is reported to the AP. This is a standard beam management step for both 3GPP NR [16] and IEEE 802.11ad/ay [9];
- the AP processes the report to identify the best beam to be used, as well as the Modulation and Coding Scheme (MCS) that offers the best rate for a given target error rate on the link;
- the AP forwards the report also to the proxy, together with additional information on which beam was chosen, the MCS, and the scheduling policy for coordinated transmissions. This makes the proxy aware of the data rate that can be exploited on the mmWave link, and allows the proxy to collect temporal and spatial statistics on the channel quality, that can help implement predictive policies. Moreover, the AP may also share statistics on the buffering delays in its internal queues, if any. The reporting is done every time the Bandwidth-Delay Product (BDP) estimate changes, with the aim of minimizing the communication overhead.

Moreover, contrary to [33], in this work we consider a private network deployment, in which all the equipment involved in the end-to-end flow is under the control of the private network operator (e.g., the factory owner). This is a typical scenario in the context of factory automation, as discussed in [36]. In this configuration, the proxy can use custom control messages to interact with the TCP stack and the AP, to perform the aforementioned procedure and, for example, gather statistics on the Round Trip Time (RTT) of the different end-to-end flows. Another deployment option in which the proxy can perform the same tasks is the traditional split configuration, in which the end-to-end connection is divided into two separate flows and the proxy optimizes the performance in the network portion towards the mobile device.

Therefore, the proxy can collect the following information across the different layers of the protocol stack:

- the matrix \mathbf{B}_t of the SNR for each beam at time t , and the past matrices $\mathbf{B}_{t-i}, i \geq 1$, together with the list of beam pairs selected by the AP and mobile device. An example of \mathbf{B}_t is shown in Fig. 2 for the office scenario depicted in Fig. 5b, described in Sec. V;
- the MCS M currently used for the communication. The MCS usually takes discrete values (e.g., for IEEE 802.11ad it ranges from 0 to 31 [7]). Each value corresponds to a modulation and a coding rate, and thus can be mapped to a spectral efficiency s and, eventually, to the available data rate $R = sB$, with B the bandwidth allocated to the user;
- the minimum round-trip time T of the flow that the proxy aims at optimizing.

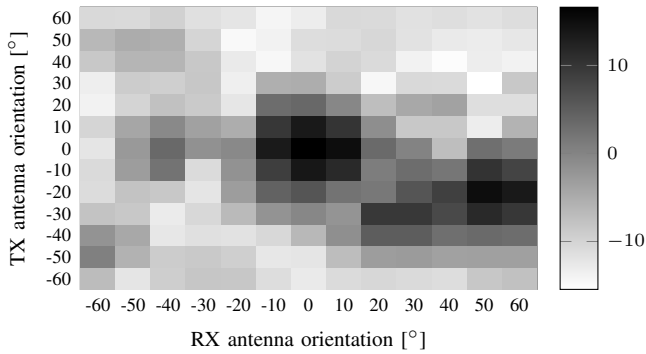


Fig. 2: Example of SNR reporting with the matrix \mathbf{B}_t , with the receiver (transmitter) antenna orientation on the x (y) axis.

A. Proxy policies

The proxy exploits the information described in the previous paragraphs to enact different flow control policies and steer the congestion window of the TCP server. In particular, we propose two different policies: (i) a reactive strategy, in which the proxy follows the dynamics of the channel and adapts accordingly; and (ii) a proactive strategy, in which the proxy tries to anticipate the evolution of the channel and possible drops in the available capacity. With both options, the proxy only modifies the value of the congestion window, while the legacy congestion awareness mechanisms (i.e., based on Duplicate Acknowledgment (DUPACK) and Retransmission Time-Out (RTO) events) are left to the TCP stack in the server [30]. In this way, the overall transport protocol operations are robust against the packet loss (thanks to the retransmissions of TCP) and the erratic behavior of the channel (thanks to the cross-layer-based congestion window selection). Finally, additional policies can be developed and implemented in the proxy, and this is left as a future extension of this work.

Reactive policy – In this case, the proxy receives the updates on the available rate R from the AP and, using its internal estimate of the RTT T , sets the congestion window C to be equal to the BDP of the flow of interest, i.e., $C = RT$. Notice that, as discussed in [24], [33], by using the minimum RTT (estimated when the system is not loaded), the BDP is not overestimated or affected by the buffering. As outlined in the previous section, the AP may also decide to generate a report for the proxy only when the estimated BDP changes: this happens, for example, when the MCS used in the communication between the AP and the mobile device changes.

Proactive policy – This scheme is similar to the reactive one, but, in addition, aims at sensing a possible imminent drop in capacity, thus giving the proxy the possibility of tuning the congestion window in advance. In this way, it is possible to reduce the excess of buffering and the increase in RTT that happens with any reactive scheme from the moment when the channel condition changes to when the proxy receives a report related to the update. Notice that, in this paper, we consider a heuristic approach, which however can be refined with a data-driven approach based on a larger set of measurements than

the one we will introduce in Section IV.

The algorithm considers a window of 150 ms. If during this time interval the MCS index selected by the AMC mechanism decreases by two or more values, which is an indication of a rapid degradation of the channel quality, the algorithm enters a *conservative mode*. During this phase, the TCP stack first initializes the Time To Recover (TTR) timer, which, for the scenarios considered in Section V, is set to 0.8 s. Then, for this entire duration, the congestion window remains set to a value equivalent to the minimum BDP, corresponding to the lowest-rate MCS, which protects the communication using the highest level of redundancy. This guarantees a conservative estimate of the capacity until the TTR expires. Once the TCP stack exits the conservative mode, the algorithm checks if the congestion window can be increased using the BDP estimate: however, in order to avoid a sudden increase of packets that flow into the network (which would eventually lead to congested buffers), the proactive policy also ensures that the congestion window is increased gradually. If after the conservative mode the channel is still in a bad condition, the algorithm continues to rely on its conservative policies. In case an outage is experienced (i.e., temporary or permanent link breakage), the scheme interrupts the communication as long as the outage persists. It has to be further highlighted that the algorithm remains in conservative mode for the whole duration of the interval corresponding to the TTR, even if the channel is able to recover before the timer expires. Moreover, notice that the conservative mode does not replace the acknowledgments-based recovery procedures (e.g., fast retransmission) that are implemented in the traditional versions of TCP. This policy is more conservative than the reactive one, thus, as we will discuss in Section V, there exists a tradeoff between the achievable throughput and the latency experienced at the application layer.

IV. EXPERIMENTAL AND SIMULATION SETUP

This section describes the setup we used to collect the channel traces to be used in the performance evaluation. The channel measurements (in terms of received power) have been carried out with a software-defined experimental testbed, based on Field Programmable Gate Array (FPGA) boards and Radio Frequency (RF) equipment configured to work at mmWave frequencies. Each FPGA generates and modulates the digital signal representing data to transmit, which is then converted from digital to analog and up-converted to a 60 GHz carrier to be fed to a transmitting antenna.

The platform provides access to detailed information regarding the implemented hardware, such as for example:

- the antenna radiation patterns and the link budget;
- all the physical layer parameters (e.g., modulation type, code rate, data rate) regarding each implemented MCS.

The high level of access to the experimental platform details has been fundamental to understand the behavior of the 60 GHz channel in the scenarios of interest. For example, the information on the received power and the antenna patterns makes it possible to understand if the endpoints are communicating using the LOS path or through reflections.

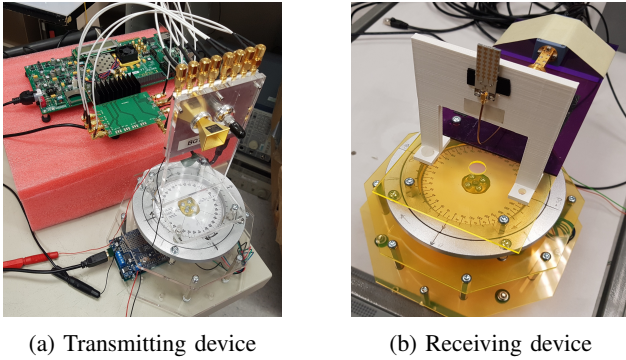


Fig. 3: Software-defined platform for the collection of the channel traces.

In a first calibration phase, we measured the Modulation Error Ratio (MER) of actual digitally modulated transmissions [37]. We performed these measurements on both LOS and NLOS scenarios, where the reflections make the communication possible even without the direct path [38]. It has to be highlighted that, in this context, the term *path* refers to a particular combination of directions towards which the transmitter and receiver steer their antennas, measured by the angle between the antennas and a plane of reference [39]. Each single MER measurement is in fact associated to a pair of values representing the transmitter and receiver directions.

After collecting calibration data, the second measurement phase focused on the received power from a continuous wave (CW). Since the setup for this new type of measurement could give us a more precise insight on the communication link and was easier to reproduce and automate, we decided to conduct all the campaigns using the testbed designed as follows:

- at the transmitter side, the FPGA is equipped with a 20-dBi horn antenna with 14° half-power beamwidth in the E-plane and 15° beamwidth in the H-plane, configured to transmit a 60 GHz CW, as shown in Figure 3a;
- at the receiver side, we connected a spectrum analyzer to a 17-dBi 32-element patch array with 24° half-power beamwidth in the E-plane and 11° beamwidth in the H-plane, reported in Figure 3b, in order to directly obtain the power of the CW, measured in dBm.

Both the transmitting and the receiving antennas were equipped with a rotating platform automatically programmed to span an interval of directions using a pre-determined angle step of 10° ; in addition, the acquisition procedure has been automated, in order to remove the systematic errors that could be introduced by the human operator. The output of this procedure corresponds to a matrix of values, each point representing the power measured using a specific combination of directions at the transmitter and the receiver. Notice that, for the results in Sec. V, we consider an angular space of $[-30^\circ, 30^\circ]$ at both endpoints.

This process was repeated for all the scenarios of interest, such as the cubicle isle of an office area and the laboratory room with different sources of reflections. In addition, starting from a specific value of CW we devised a step-by-step algo-

rithm to calculate the corresponding MER, which is needed for the Block Error Rate (BLER) and MCS computation with link-to-system mapping (LSM) techniques. In the following we detail each step of the algorithm, starting from the theoretical assumptions in Sec. IV-A, down to the implementation of the Link-to-System mapping in Sec. IV-B and the description of the simulated network infrastructure.

A. Theoretical Assumptions and Data Preprocessing

Assuming to work at room temperature T_0 (300 K) using the same bandwidth of 500 MHz used to estimate the MER, we modeled the noise as Additive White Gaussian Noise (AWGN) [40]. Considering that the power of the CW is measured over a narrow bandwidth, we assume that the transceivers considered in our system can transmit and sense without distortions in the entire bandwidth. Then, applying the following formula

$$P_{noise}^{CW} = 10 \log(N_0 B) + 30 \text{ [dBm]}, \quad (1)$$

we obtain a value of $P_{noise}^{CW} = -87.01$ dBm. Substituting this value in the following equation:

$$SNR_{RX}^{CW} = P_{RX}^{CW} - P_{noise}^{CW} \text{ [dB]} \quad (2)$$

we can assess the SNR at the input of the receiver.

Since Eq. (2) represents the noise-ratio up to the receiving antenna, we can express the MER as the SNR plus an additional noise introduced by the demodulation chain. This value can then be calculated as:

$$\Delta = SNR_{RX}^{CW} - MER_{RX}^{FPGA} \text{ [dB]}, \quad (3)$$

where MER_{RX}^{FPGA} is the value of MER¹, expressed in dB, measured at the input of the receiving FPGA board. Moreover, the measured value of MER can be affected by several issues [37]:

- *statistical variation*, which depends on the number of samples N ; a smaller standard deviation (in general proportional to $\frac{1}{\sqrt{N}}$) means that the MER will appear more stable.
- *nonlinear effects*, in particular on outer constellation points. It is of fundamental importance that we measure the same constellation that will be used for transmitting data; moreover, the captured sample of data must be long enough to ensure that all symbols occur with equal likelihood.
- *MER saturation*, which consists in the saturation of MER at a value reflecting the implementation loss of the receiver, consisting for example in wrong symbol decoding, due to symbol detector inefficiency.

Based on our laboratory experiments, we found that above a certain threshold the receiver front-end faces a saturation problem; this means that, even if the received power increases, the board could not yield a higher precision/lower error when demodulating the signal into a value of the constellation. For this reason we decided to set Δ to its mean value of 6.5 dB,

¹Notice that the MER is the equivalent of the SNR in the digital domain, thus takes into account the imperfections of the demodulation chain.

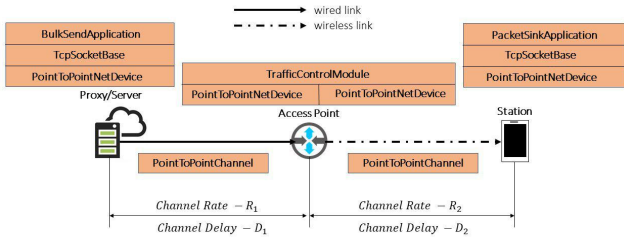


Fig. 4: Network topology used in the simulation campaigns.

obtained from an extensive measurement campaign. It must be noted that the simulator module accepts Δ as a tunable parameter, in case further experiments will supply a different value.

B. Link-To-System Mapping

In order to map the MER to the channel capacity and BLER for the wireless link, we designed an ad hoc platform to model the PHY layer, following the IEEE 802.11ad standard [7]. This module implements the procedure described in [41], which specifies for IEEE 802.11ad the approach adopted in [42].

Using a suitable value of Mean Mutual Information per coded Bit (MMIB), we can evaluate the BLER as:

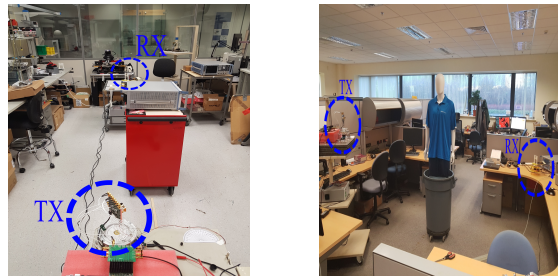
$$BLER = \frac{1}{2} \left[1 - \operatorname{erf} \left(\frac{MMIB - X_1}{\sqrt{2}X_2} \right) \right], \quad X_2 \neq 0 \quad (4)$$

where X_1 and X_2 depend on the modulation order considered.

The complete process is the following: (i) first a value of CW power is converted to the corresponding value of MER; then (ii) the algorithm spans the MCS space to find the highest value that satisfies the BLER constraint (maximum value tolerated for the wireless link), for which the actual channel BLER is evaluated as a function of MER and the MCS under study. The available MCS and error rate obtained through this step-by-step procedure are assigned to the wireless channel; following previous assumptions, the channel capacity is evaluated using the spectral efficiency associated to the chosen MCS, assuming a 500 MHz bandwidth [41]. Based on the MCS obtained, the devices could generate channel reports, according to which congestion policy is implemented as described in Section III.

C. Simulated Architecture

The scenario described in Figure 1 is implemented in ns-3 using the LSM abstraction of Section IV-B and the two-link network topology reported in Figure 4. In this evaluation, we consider a single-user scenario. The first link includes the TCP proxy and the AP, which are connected using a wired link with fixed channel rate and a communication latency of 20 ms. The second link connects the same AP, which acts as gateway, to a receiving mobile device using a wireless link. In the following, all the modules, classes and functions that we are going to mention either are part of the ns-3 simulator's core [43], [44] or have been designed and written during our study.



(a) Scenario A.

(b) Scenario B.

Fig. 5: Framework of the measurement campaign.

As shown in Fig. 4, each node has installed a `PointToPointNetDevice` and the links between the nodes have been emulated using two distinct instances of the `PointToPointChannel` class. Since the `PointToPointChannel` does not implement any propagation loss model by default, we designed an additional module in order to associate the measured traces to the wireless link. The module consists of two main classes:

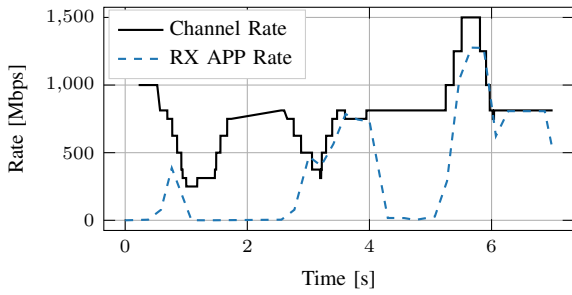
- `MmWavePhyAbstraction`, which lists the methods and attributes used to manage the LSM described in Section IV-B;
- `MmWaveChannelTracker` which deals with the input preprocessing and provides the functions that update the wireless channel. It also manages the report infrastructure between the mobile device, the AP and the proxy (along with the communication with the TCP socket).

The application server continuously generates packets using `BulkSendApplication` with the aim of keeping the TCP sending socket buffer filled. In this way the communication is not limited by the application behavior, and is supervised by the policies of flow and congestion control implemented in TCP. An instance of `PacketSinkApplication` is installed in the receiving mobile device, which relies on the TCP socket for the acknowledgment procedures. The AP further implements a `TrafficControlModule`, provided by ns-3 and configured to use a queue implementing a Priority First In First Out (PFIFO) policy.

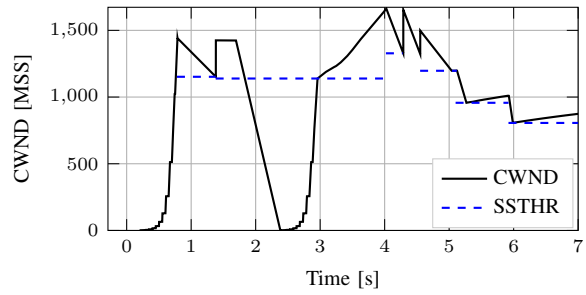
It is important to highlight that in our simulations we considered only MCS from 1 to 12, corresponding to the Single Carrier (SC) mode; in addition, as described in [41], in order to reach a maximum channel rate of 1.5 Gbps, at the application layer we create packets of 8140 Bytes. This version of the simulator, in fact, does not provide strategies of frame aggregation at the MAC layer. Also, link-layer retransmission policies have not been considered, since this study is focused on studying the performance of TCP also in case of erratic mmWave channel behavior and loss events. Nevertheless, this will be considered in future updates of the simulator.

V. PERFORMANCE EVALUATION

The first scenario (A) we consider in this evaluation is shown in Figure 5a, with the antennas positioned at a height of 1 m and at a distance of 3 m from each other. During

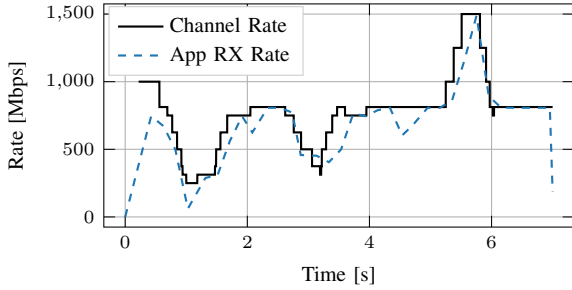


(a) Channel and application rate

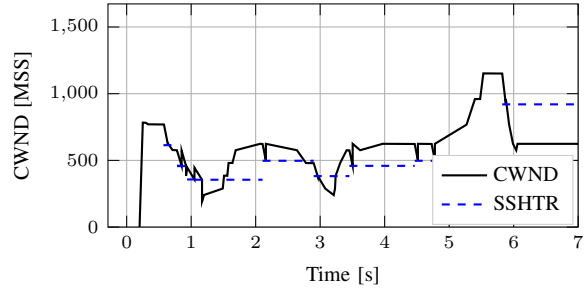


(b) Congestion window and slow start threshold

Fig. 6: Performance of the baseline TCP CUBIC congestion control in Scenario B.



(a) Channel and application rate



(b) Congestion window and slow start threshold

Fig. 7: Performance of the proxy-based reactive congestion control in Scenario B.

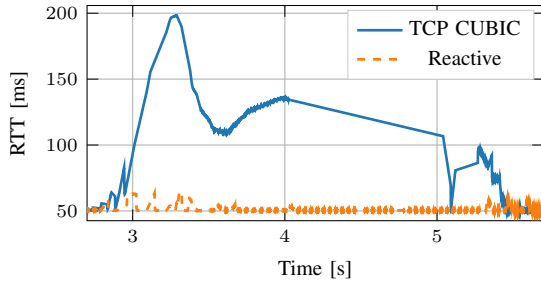


Fig. 8: Latency comparison between baseline and reactive policy in Scenario B.

the measurements, a trolley is moved along a straight line in a perpendicular direction with respect to the communication path, using a 0.2 m step. Measurements as described in Sec. IV are taken periodically and then interpolated to create a dynamic blockage trace. In this environment, the presence of several reflectors easily provides an alternative to the main, blocked, LOS path.

In the second scenario (B), shown in Fig. 5b, the two antennas communicate from the opposite angles of a cubicle isle: the receiver was positioned on top of a desk at a 1 m height, while the transmitter was at a height of 1.6 m, at a distance of 3.5 m. In this case the LOS was obstructed with a manikin of 1.9 m of height, filled with salty water in order to experience an attenuation comparable to that of a real human being; this setup is similar to a typical indoor communication where, even if there is no blockage in the environment, there

is no direct LOS path available due to the different height of the devices. In this case, the blockage moved at a speed of 0.1 m/s.

As an example, a comparison between the baseline congestion control mechanism (i.e., TCP CUBIC, the default congestion control in the Linux kernel) and the reactive policy described in Sec. III-A is shown in Figures 6 and 7, respectively, for scenario B. In particular, Figure 6a highlights that the channel quality and, consequently, the available data rate at the physical layer continuously vary as the manikin moves between the two transceivers. Under these challenging conditions, the beam selection algorithm has to switch several times from one antenna sector to the other, to find the one that yields the highest received power. As we expected, the main difference is represented by the trend of the Congestion Window (CWND) of the two schemes. TCP CUBIC tries to infer the channel behavior from packet loss events but, by doing so, overestimates the CWND and (a) causes a massive buffer overflow, which translates into the RTO event at ~ 2 s in Fig. 6, and (b) generally yields a poor match between the wireless link capacity and the application layer throughput, which drops to rates smaller than 10 Mbps for extended intervals, as shown in Fig. 6a. Our reactive policy, instead, aims at exploiting the channel at its full capacity. Therefore, in the proxy-based scheme the CWND reflects the trend of the channel rate, as illustrated in Fig. 7a, so that the receiving application is able to achieve the rate offered by the mmWave link.

This also makes it possible to control the latency measured

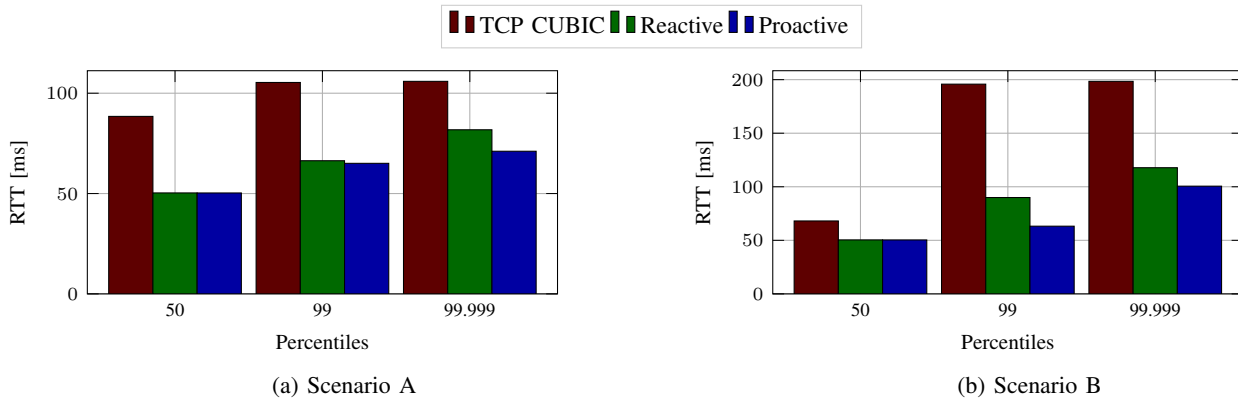


Fig. 9: RTT percentiles (50, 99, 99.999) in the two scenarios of interest.

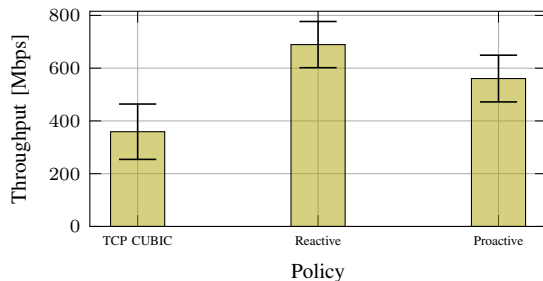


Fig. 10: Average throughput at the application layer from scenarios A and B, C.I. 95%.

at the application layer, which is shown in Figure 8 for both schemes. In particular, the results focus on an interval of time corresponding to one of the blockage events: while TCP CUBIC is affected by a high latency, due to the long queues in the buffers of the network, our scheme copes with the changes in capacity and guarantees an RTT not higher than 70 ms (with respect to the peak of 200 ms experienced by TCP CUBIC).

Figure 9 reports the latency (i.e., the RTT) for both scenarios, evaluated at different percentiles, from the median, to the worst 0.001% of the received packets (i.e., those representing the high tail of the latency distribution of the $\sim 10^6$ simulated packets). In both scenarios it is possible to observe a reduction of up to 50% in the experienced RTT. An additional latency reduction is obtained by using a proactive approach, which, as discussed in Sec. III, makes the proxy more conservative during the intervals in which the channel is blocked, with an improvement especially on the worst percentiles. This advantage from the point of view of latency, however, comes at the cost of a lower average throughput with respect to the reactive scheme, as shown in Fig. 10 (obtained by averaging the results from both scenarios). This introduces a trade-off between achievable application rate and latency, and whether to prefer one or the other largely depends on the QoS constraints dictated by the specific application.

VI. CONCLUSIONS

In this work, we introduced a novel proxy-based approach to control and improve the performance of TCP over mmWave links, which, as discussed, is affected by high latency spikes

and low throughput due to the erratic behavior of the channel. We proposed two congestion control policies, where the congestion window of the TCP sender is updated according to estimates of the Round Trip Time and Bandwidth-Delay Product. Moreover, we evaluated the performance of the proposed solution using real channel traces, collected in a number of different indoor scenarios, and fed to a custom ns-3 extension that simulates the IEEE 802.11ad physical layer.

In general, the policies that we designed outperform legacy congestion control strategies, from the point of view of both latency (compared in terms of percentiles) and average throughput (evaluated at the application layer). Moreover, we determined that the choice between our two proposed schemes must be made based on the application of interest.

These improvements come at the cost of a new specific architecture (i.e., a proxy that splits the connections) to be implemented, able to manage different transmission flows while covering all kinds of network situations. Solutions that include multiple mobile devices and access points in the same network will be considered as possible future works. Moreover, future studies will further investigate the proactive policy, using a data-driven approach.

REFERENCES

- [1] Cisco, “Cisco Visual Networking Index: Forecast and Trends, 2017–2022,” *White Paper*, 2018.
- [2] Q. Wang and J. Jiang, “Comparative Examination on Architecture and Protocol of Industrial Wireless Sensor Network Standards,” *IEEE Communications Surveys & Tutorials*, vol. 18, no. 3, pp. 2197–2219, Third quarter 2016.
- [3] G. Berardinelli, N. H. Mahmood, I. Rodriguez, and P. Mogensen, “Beyond 5G Wireless IRT for Industry 4.0: Design Principles and Spectrum Aspects,” in *IEEE Globecom Workshops (GC Wkshps)*, Dec 2018.
- [4] M. Khoshnevisan, V. Joseph, P. Gupta, F. Meshkati, R. Prakash, and P. Tinnakornsrisuphap, “5G Industrial Networks With CoMP for URLLC and Time Sensitive Network Architecture,” *IEEE Journal on Selected Areas in Communications*, vol. 37, no. 4, pp. 947–959, April 2019.
- [5] S. Rangan, T. S. Rappaport, and E. Erkip, “Millimeter-Wave Cellular Wireless Networks: Potentials and Challenges,” *Proceedings of the IEEE*, vol. 102, no. 3, pp. 366–385, March 2014.
- [6] 3GPP, “NR and NG-RAN Overall Description - Rel. 15,” TS 38.300, 2018.
- [7] IEEE, “IEEE Standard for Information Technology–Telecommunications and Information Exchange between Systems–Local and Metropolitan Area Networks–Specific Requirements–Part 11: Wireless LAN Medium

- Access Control (MAC) and Physical Layer (PHY) Specifications Amendment 3: Enhancements for Very High Throughput in the 60 GHz Band," *IEEE Std 802.11ad-2012 (Amendment to IEEE Std 802.11-2012, as amended by IEEE Std 802.11ae-2012 and IEEE Std 802.11aa-2012)*, pp. 1–628, Dec 2012.
- [8] —, "IEEE Draft Standard for Information Technology–Telecommunications and Information Exchange Between Systems Local and Metropolitan Area Networks–Specific Requirements Part 11: Wireless LAN Medium Access Control (MAC) and Physical Layer (PHY) Specifications–Amendment: Enhanced Throughput for Operation in License-Exempt Bands Above 45 GHz," *IEEE Draft Std P802.11ay (Amendment to IEEE Std 802.11-2012, as amended by IEEE Std 802.11ae-2012 and IEEE Std 802.11aa-2012)*, 2019.
- [9] C. Pielli, T. Ropitault, and M. Zorzi, "The potential of mmwaves in smart industry: Manufacturing at 60 ghz," in *Ad-hoc, Mobile, and Wireless Networks*. Springer International Publishing, 2018, pp. 64–76.
- [10] S. Saponara, F. Giannetti, B. Neri, and G. Anastasi, "Exploiting mm-Wave Communications to Boost the Performance of Industrial Wireless Networks," *IEEE Transactions on Industrial Informatics*, vol. 13, no. 3, pp. 1460–1470, June 2017.
- [11] Z. Pi and F. Khan, "An introduction to millimeter-wave mobile broadband systems," *IEEE Communications Magazine*, vol. 49, no. 6, June 2011.
- [12] V. Raghavan, L. Akhoondzadeh-Asl, V. Podshivalov, J. Hulten, M. A. Tassoudji, O. H. Koymen, A. Sampath, and J. Li, "Statistical Blockage Modeling and Robustness of Beamforming in Millimeter-Wave Systems," *IEEE Transactions on Microwave Theory and Techniques*, vol. 67, no. 7, pp. 3010–3024, July 2019.
- [13] J. S. Lu, D. Steinbach, P. Cabrol, and P. Pietraski, "Modeling human blockers in millimeter wave radio links," *ZTE Communications*, vol. 10, no. 4, pp. 23–28, 2012.
- [14] G. R. MacCartney, T. S. Rappaport, and S. Rangan, "Rapid Fading Due to Human Blockage in Pedestrian Crowds at 5G Millimeter-Wave Frequencies," in *IEEE Global Communications Conference (GLOBECOM)*, Dec 2017, pp. 1–7.
- [15] S. Akoum, O. El Ayach, and R. W. Heath, "Coverage and capacity in mmwave cellular systems," in *46th Asilomar Conference on Signals, Systems and Computers*. IEEE, 2012, pp. 688–692.
- [16] M. Giordani, M. Polese, A. Roy, D. Castor, and M. Zorzi, "A Tutorial on Beam Management for 3GPP NR at mmWave Frequencies," *IEEE Communications Surveys & Tutorials*, vol. 21, no. 1, pp. 173–196, First quarter 2019.
- [17] M. Polese, M. Giordani, M. Mezzavilla, S. Rangan, and M. Zorzi, "Improved Handover Through Dual Connectivity in 5G mmWave Mobile Networks," *IEEE Journal on Selected Areas in Communications*, vol. 35, no. 9, pp. 2069–2084, Sept 2017.
- [18] H. Shokri-Ghadikolaie, C. Fischione, G. Fodor, P. Popovski, and M. Zorzi, "Millimeter Wave Cellular Networks: A MAC Layer Perspective," *IEEE Transactions on Communications*, vol. 63, no. 10, pp. 3437–3458, Oct 2015.
- [19] M. Zhang, M. Mezzavilla, R. Ford, S. Rangan, S. Panwar, E. Mellios, D. Kong, A. Nix, and M. Zorzi, "Transport layer performance in 5G mmWave cellular," in *IEEE Conference on Computer Communications Workshops (INFOCOM WKSHPs)*, April 2016, pp. 730–735.
- [20] M. Zhang, M. Polese, M. Mezzavilla, J. Zhu, S. Rangan, S. Panwar, and a. M. Zorzi, "Will TCP Work in mmWave 5G Cellular Networks?" *IEEE Communications Magazine*, vol. 57, no. 1, pp. 65–71, January 2019.
- [21] M. Polese, R. Jana, and M. Zorzi, "TCP and MP-TCP in 5G mmWave Networks," *IEEE Internet Computing*, vol. 21, no. 5, pp. 12–19, Sep. 2017.
- [22] J. Gettys and K. Nichols, "Bufferbloat: Dark buffers in the internet," *ACM Queue*, vol. 9, no. 11, pp. 40:40–40:54, Nov 2011.
- [23] S. Sur, I. Pefkianakis, X. Zhang, and K.-H. Kim, "WiFi-Assisted 60 GHz Wireless Networks," in *Proc. of ACM MobiCom*, Snowbird, Utah, USA, 2017, pp. 28–41.
- [24] M. Zhang, M. Mezzavilla, J. Zhu, S. Rangan, and S. Panwar, "Tcp dynamics over mmwave links," in *IEEE 18th International Workshop on Signal Processing Advances in Wireless Communications (SPAWC)*, July 2017, pp. 1–6.
- [25] A. Kessler and M. Pieskä, "TCP Performance over 5G mmWave Links-Tradeoff between Capacity and Latency," in *13th IEEE International Conference on Wireless and Mobile Computing, Networking and Communications*, 2017, pp. 385–394.
- [26] M. Polese, M. Mezzavilla, S. Rangan, and M. Zorzi, "Mobility Management for TCP in mmWave Networks," in *Proceedings of the 1st ACM Workshop on Millimeter-Wave Networks and Sensing Systems, collocated with ACM MobiCom'17*, ser. mmNets '17, 2017, pp. 11–16.
- [27] M. Mezzavilla, M. Zhang, M. Polese, R. Ford, S. Rangan, and M. Zorzi, "End-to-End Simulation of 5G mmWave Networks," *IEEE Communications Surveys & Tutorials*, vol. 20, no. 3, pp. 2237–2263, Third quarter 2018.
- [28] S. K. Saha, A. Garg, and D. Koutsonikolas, "A first look at TCP performance in indoor IEEE 802.11ad WLANs," in *IEEE Conference on Computer Communications Workshops (INFOCOM WKSHPs)*, Apr 2015, pp. 63–64.
- [29] S. Ha, I. Rhee, and L. Xu, "CUBIC: a new TCP-friendly high-speed TCP variant," *ACM SIGOPS Operating Systems Review*, vol. 42, no. 5, pp. 64–74, July 2008.
- [30] T. Henderson, S. Floyd, A. Gurtov, and Y. Nishida, "The NewReno Modification to TCP's Fast Recovery Algorithm," RFC 6582, 2012.
- [31] V. S. Chakravarthi and S. Burli, "Architecting 802.11ad WLAN SoC for best performance," in *IEEE Region 10 Conference (TENCON)*, Nov 2016, pp. 3554–3558.
- [32] 3GPP, "Radio Link Control (RLC) protocol specification - Rel. 15," TS 38.322, 2018.
- [33] M. Polese, M. Mezzavilla, M. Zhang, J. Zhu, S. Rangan, S. Panwar, and M. Zorzi, "milliProxy: A TCP proxy architecture for 5G mmWave cellular systems," in *51st Asilomar Conference on Signals, Systems, and Computers*, Oct 2017, pp. 951–957.
- [34] M. Kim, S. W. Ko, and S. L. Kim, "Enhancing TCP end-to-end performance in millimeter-wave communications," in *IEEE 28th Annual International Symposium on Personal, Indoor, and Mobile Radio Communications (PIMRC)*, Oct 2017.
- [35] T. Azzino, M. Drago, M. Polese, A. Zanella, and M. Zorzi, "X-TCP: a cross layer approach for TCP uplink flows in mmwave networks," in *16th Annual Mediterranean Ad Hoc Networking Workshop (Med-Hoc-Net)*, June 2017.
- [36] M. Wollschlaeger, T. Sauter, and J. Jasperneite, "The Future of Industrial Communication: Automation Networks in the Era of the Internet of Things and Industry 4.0," *IEEE Industrial Electronics Magazine*, vol. 11, no. 1, pp. 17–27, March 2017.
- [37] R. Hranac, "Digital transmission: Carrier-to-noise ratio, signal-to-noise ratio, and modulation error ratio," *Broadcom Corporation and Cisco Systems, white paper*, 2006.
- [38] T. S. Rappaport, S. Sun, R. Mayzus, H. Zhao, Y. Azar, K. Wang, G. N. Wong, J. K. Schulz, M. Samimi, and F. Gutierrez, "Millimeter wave mobile communications for 5G cellular: It will work!" *IEEE access*, vol. 1, pp. 335–349, 2013.
- [39] M. R. Akdeniz, Y. Liu, M. K. Samimi, S. Sun, S. Rangan, T. S. Rappaport, and E. Erkip, "Millimeter wave channel modeling and cellular capacity evaluation," *IEEE Journal on Selected Areas in Communications*, vol. 32, no. 6, pp. 1164–1179, June 2014.
- [40] R. K. Mueller and G. J. Foschini, "The capacity of linear channels with additive gaussian noise," *The Bell System Technical Journal*, vol. 49, no. 1, pp. 81–94, Jan 1970.
- [41] A. Maltsev, A. Pudneyev, I. Bolotin, G. Morozov, I. Karls, M. Faerber, I. Siaud, A. Ulmer-Moll, J. Conrat, R. Weiler *et al.*, "Miweba d4. 1: System level simulator specification," *Millimeter-wave evolution for backhaul and access (MiWEBA) project*. Available: <http://www.miweba.eu>, 2014.
- [42] M. Mezzavilla, M. Miozzo, M. Rossi, N. Baldo, and M. Zorzi, "A lightweight and accurate link abstraction model for the simulation of LTE networks in ns-3," in *Proceedings of the 15th ACM international conference on Modeling, analysis and simulation of wireless and mobile systems*. ACM, 2012, pp. 55–60.
- [43] M. Casoni and N. Patriciello, "Next-generation TCP for ns-3 simulator," *Simulation Modelling Practice and Theory*, vol. 66, pp. 81 – 93, 2016. [Online]. Available: <http://www.sciencedirect.com/science/article/pii/S1569190X15300939>
- [44] T. R. Henderson, M. Lacage, G. F. Riley, C. Dowell, and J. Kopena, "Network simulations with the ns-3 simulator," *SIGCOMM demonstration*, vol. 14, no. 14, p. 527, 2008.